Research Article

NMR IN BIOMEDICINE

Received: 13 July 2009, Revised: 20 April 2010, Accepted: 21 April 2010, Published online in Wiley Online Library: 6 September 2010

(wileyonlinelibrary.com) DOI:10.1002/nbm.1568

MRI of stroke using hyperpolarized ^{129}Xe

Xin Zhou[a,b]*, Yanping Sun[b,c], Mary Mazzanti[b,c], Nils Henninger[d], Joey Mansour[b,c], Marc Fisher[d] and Mitchell Albert[b,c]

Because there is no background signal from xenon in biological tissue, and because inhaled xenon is delivered to the brain by blood flow, we would expect a perfusion deficit, such as is seen in stroke, to reduce the xenon concentration in the region of the deficit. Thermal polarization yields negligible xenon signal relative to hyperpolarized xenon; therefore, hyperpolarized xenon can be used as a tracer of cerebral blood flow. Using a rat permanent right middle cerebral artery occlusion model, we demonstrated that hyperpolarized ^{129}Xe MRI is able to detect, *in vivo*, the hypoperfused area of focal cerebral ischemia, that is the ischemic core area of stroke. To the best of our knowledge, this is the first time that hyperpolarized ^{129}Xe MRI has been used to explore normal and abnormal cerebral perfusion. Our study shows a novel application of hyperpolarized ^{129}Xe MRI for imaging stroke, and further demonstrates its capacity to serve as a complementary tool to proton MRI for the study of the pathophysiology during brain hypoperfusion. Copyright © 2010 John Wiley & Sons, Ltd.

Keywords: hyperpolarized ^{129}Xe; stroke MRI; rat brain; infarct

INTRODUCTION

Stroke is the third leading cause of death in developed countries and is the single most common reason for permanent disability. In the USA, about 780,000 people suffer from stroke every year, leading to 150,000 deaths, and the estimated direct and indirect costs associated with stroke for 2008 totaled $65.5 billion (1). During acute ischemic stroke, a core of brain cells at the center of the affected region dies quickly, and the damage subsequently spreads to surrounding tissue over the next several hours (2). Because they allow for the delineation of areas of ischemic neuronal injury and hypoperfusion within minutes after the induction of cerebral ischemia, conventional proton MRI, especially diffusion-weighted imaging (DWI) (3,4) and perfusion-weighted imaging (PWI) (5,6), have been particularly useful in the diagnosis of acute ischemic stroke.

The target of acute stroke therapy is the portion of the ischemic region that is still potentially salvageable, that is the ischemic penumbra (7). MRI operationally defines the ischemic penumbra by the PWI–DWI mismatch area. DWI detects changes in the apparent diffusion coefficient (ADC) of water molecules associated with early cytotoxic edema in ischemic stroke. Arterial spin labeling (ASL)-based PWI methods provide excellent anatomical information for the measurement of tissue perfusion (5). The ASL technique shows numerous advantages, such as noninvasive measurements of cerebral blood flow (CBF) quantifiable in standard units of mL/g/min, and is able to image multi-slices and multi-regions of the brain. However, in some situations, PWI methods require the injection of gadolinium-containing contrast agents to map relative CBF in order to identify the hypoperfused tissue (8–11). In addition to the conventional DWI and PWI techniques, van Zijl and coworkers (12,13) have developed pH-weighted MRI to study stroke and ischemic penumbra. However, proton imaging has a large background signal in biological tissue, and contrast injection is an invasive approach. Moreover, contrast-associated nephrogenic systemic fibrosis has been reported after the use of gadolinium-based agents, and many patients with impaired renal function are not eligible to receive contrast media (14–17).

In contrast, hyperpolarized ^{129}Xe MRI shows great potential and advantages for the identification of hypoperfused brain tissue. Xenon is highly lipid soluble and lacks an intrinsic background signal in biological tissue (18). Duhamel *et al*. (19,20) have studied CBF using intra-arterial injection of hyperpolarized ^{129}Xe dissolved in a lipid emulsion. Alternatively, hyperpolarized ^{129}Xe can be administered noninvasively by inhalation; following inhalation, ^{129}Xe is absorbed into the bloodstream and delivered to the brain through the circulation. Because the spin-exchange optical pumping technique can enhance the ^{129}Xe MR signal 10,000–100,000 times over thermal polarization (21–23), the

* *Correspondence to: X. Zhou, Wuhan Institute of Physics and Mathematics, Chinese Academy of Sciences, Wuhan 430071, China.*
E-mail: dr.xin.zhou@gmail.com, xinzhou@wipm.ac.cn

a *X. Zhou*
State Key Laboratory of Magnetic Resonance and Atomic and Molecular Physics, Wuhan Center for Magnetic Resonance, Wuhan Institute of Physics and Mathematics, Chinese Academy of Sciences, Wuhan, China

b *X. Zhou, Y. Sun, M. Mazzanti, J. Mansour, M. Albert*
Department of Radiology, Brigham and Women's Hospital, Harvard Medical School, Boston, MA, USA

c *Y. Sun, M. Mazzanti, J. Mansour, M. Albert*
Department of Radiology, University of Massachusetts Medical School, Worcester, MA, USA

d *N. Henninger, M. Fisher*
Department of Neurology, University of Massachusetts Medical School, Worcester, MA, USA

Abbreviations used: *ADC, apparent diffusion coefficient; ASL, arterial spin labeling; CBF, cerebral blood flow; CCA, common carotid artery; CSI, chemical shift imaging/image; DWI, diffusion-weighted imaging; ICA, internal carotid artery; MCAO, middle cerebral artery occlusion; PWI, perfusion-weighted imaging; ROI, region of interest; S_pO_2, peripheral oxygen saturation; TTC, 2,3,5-triphenyltetrazolium chloride.*

NMR IN BIOMEDICINE

dissolved-phase hyperpolarized ^{129}Xe signal in the brain can be detected even at low concentrations. Because the xenon signal is proportional to CBF (24), a decrease in the signal is expected to occur in areas of decreased CBF after the inhalation of hyperpolarized xenon gas. Hyperpolarized xenon imaging currently cannot achieve a slice as thin as that obtained by ASL. In addition, ASL can be performed with substantially higher spatial resolution than hyperpolarized xenon imaging in brain tissue. However, the ASL technique requires two experiments (arterial spin labeled and controlled) to obtain CBF information. In this article, we report, for the first time, that hyperpolarized ^{129}Xe MRI is able to detect areas of decreased CBF following middle cerebral artery occlusion (MCAO) in a single scan. These findings show the great potential and utility of hyperpolarized ^{129}Xe MRI for stroke imaging, and further demonstrate that hyperpolarized ^{129}Xe is a safe and noninvasive signal source for imaging diseases and function of the brain.

MATERIALS AND METHODS

Animal preparation

All animal procedures were approved by the Harvard Medical Area Standing Committee on Animals. Eight male Sprague-Dawley rats (*Rattus norvegicus*), weighing 175–200 g, were anesthetized with isoflurane (5% for induction, 2% for surgery, 1.2% for maintenance) in room air, and no other anesthetics or paralytics were used. Permanent MCAO ($n = 4$) was produced by intraluminal suture occlusion of the right middle cerebral artery using 4-0 silicon-coated monofilament sutures, as described previously (25,26). Briefly, an occluder was introduced through the right common carotid artery (CCA) into the internal carotid artery (ICA), and then advanced approximately 18–20 mm from the CCA bifurcation until mild resistance indicated correct placement of the filament tip (27). Two control animals received sham surgery without occlusion of the middle cerebral artery. Two animals were excluded, as no xenon signal was detected during the acquisition phase because of technical issues. Following endotracheal intubation with a 14-gauge, 3.5-cm catheter, we placed the animals in the magnet and connected the catheter to an animal respirator (SAR 830 AP; CWE Inc., Ardmore, PA, USA). The respirator was interfaced to an MR-compatible gas delivery system controlled by programmed computer software (LabView; National Instruments, Austin, TX, USA). The respiratory rate was set at 60 breaths per minute and the tidal volume at 3 mL. The body temperature was maintained at $37.0 \pm 0.5^{\circ}$C using a feedback-regulated heating pad. Throughout the experiment, the animal's peripheral oxygen saturation (S_pO_2) and heart rate were monitored with a pulse oximeter (8600 V; Nonin Medical Inc., Plymouth, MN, USA) via a pair of phototransducers placed on the hind paw.

Hyperpolarized xenon gas ventilation

The xenon experimental set-up is similar to that described previously by Zhou *et al.* (24). Hyperpolarized ^{129}Xe, with a polarization of about 10%, was produced by a gas flow-through spin-exchange optical pumping polarizer (IGI.XE.2000, GE Healthcare, Durham, NC, USA); 500 mL of hyperpolarized ^{129}Xe gas was collected in 45 min. Animals were ventilated with 1.2% isoflurane in room air when ^{129}Xe chemical shift imaging (CSI) was not implemented. For 40 s prior to hyperpolarized ^{129}Xe CSI acquisition, until the xenon signal of dissolved xenon in the brain tissue reached a steady state, animals were ventilated with two breaths of room air + isoflurane alternating with two breaths of 100% hyperpolarized xenon gas (24). We then continued this ventilation protocol until after the completion of hyperpolarized ^{129}Xe CSI acquisition.

MRI

All MRI measurements were carried out on a Bruker (Ettlingen, Germany) BioSpec 4.7 T horizontal MRI system using a dual-tuned surface coil (diameter, 3.5 cm) tuned to the ^{1}H and ^{129}Xe resonance frequencies (200.1 and 55.4 MHz, respectively). We implemented shimming on the proton signal from the rat brain using an automatic shimming tool (Bruker Paravision 3.0.2). For consistent between-experiment shimming quality, we shimmed the full width at half-maximum of the hyperpolarized ^{129}Xe spectroscopy peak at 194.7 ppm to 58 Hz, which was slightly better than the normal value observed in the rat brain using a smaller surface coil (28). We acquired proton T_2-weighted images with eight slices (each slice thickness, 2.5 mm; field of view, 2.5 cm × 2.5 cm) along the axial direction to localize one specific slice, which was used for the following DWI and hyperpolarized ^{129}Xe scans. The proton ADC and hyperpolarized ^{129}Xe CSI were performed at 90 min after MCAO. We obtained the ADC map from two spin-echo images along the axial direction with two different diffusion weightings ($b = 6.070$ and 1366.159 s/mm^2), and each image was acquired over 8.5 min with a matrix of 128 × 128, TR = 2 s, TE = 35.2 ms, $\Delta = 24$ ms, $\delta = 4.75$ ms, field of view of 2.5 cm × 2.5 cm, slice thickness of 2.5 mm, one average and one slice. The diffusion gradient was only applied in a dorsal–ventral direction, that is in the same direction of frequency encoding, although the isotropically weighted diffusion technique would be better, and it is rotationally invariant (29). We acquired hyperpolarized ^{129}Xe CSI, with a chemical shift at 194.7 ppm for the major dissolved-phase tissue peak, using a slice-localized pulse sequence with free induction decay recording of signals, a sinc-shaped 90° radiofrequency pulse duration of 800 μs (the pulse power was calibrated to achieve maximal signal from the same xenon CSI slice as described below), 16 phase-encoding steps in two dimensions, each phase gradient duration of 500 μs, TR = 1 s, field of view of 2.5 cm × 2.5 cm, slice thickness of 5 mm with the slice centered at the center of the ADC slice, one average and one slice.

Histology

The rats were sacrificed 8 h following MCAO, and the brains were sectioned into axial slices (i.e. slices in the coronal or frontal plane, dividing anterior and posterior) with a slice thickness of 2.5 mm and stained with 2,3,5-triphenyltetrazolium chloride (TTC). It should be noted that, in standard medical terminology, the histology was sectioned in the rat's 'coronal' plane, but, according to standard MRI convention, this plane is referred to as the 'axial' plane; to avoid confusion, we use the MRI convention in this article.

Data analysis

We processed all the data using Matlab software (MathWorks, Natick, MA, USA). Quantitative ADC maps, in units of square millimeters per second, were calculated using the Stejskal–Tanner equation (30). The average ADC value and standard deviation of normal rat brain tissue were analyzed from a 16 × 16 region, that is a square delineated by four coordinate points, (40,

56), (56,56), (40,72) and (56,72), on the 128 × 128 ADC map. Based on previous studies characterizing the diffusion and perfusion mismatch in the MCAO model, we used the critical threshold of 5.3×10^{-4} mm^2/s to delineate the ischemia lesion core area (31). We processed raw data from xenon CSIs in spectral dimension using a 20-Hz exponential line-broadening filter, and in two phase-encoding dimensions zero-filled to 128. We then performed Fourier transforms on these three dimensions to obtain xenon CSIs (signal intensity is in arbitrary units). In order to analyze the xenon-averaged signal in different brain areas of the MCAO model, we selected two regions of interest (ROIs; shown in Fig. 3b) for statistical comparison. These ROIs describe two tissue compartments: the stroke core (ROI1), defined by a reduced ADC below the critical threshold and a TTC abnormality; normal tissue (ROI2), defined by a nonreduced (compared with the normal contralesional side) Xe CSI signal and the absence of ADC or TTC lesions.

Statistics

We present the statistical data as the mean ± one standard deviation. Statistical analysis of the physiological variables, xenon signal and lesion areas was performed using a repeated measurement analysis of variance (ANOVA). We used two-tailed Student's *t*-tests (paired or unpaired) to compare parametric variables. We set the α error level at 0.05.

RESULTS

Physiological variables (S_pO_2, heart rate) remained within normal limits throughout the experiment and there were no significant between-group differences at corresponding time points ($p > 0.05$, Table 1).

Figure 1a shows a representative axial proton image of the rat brain, and eight blue slabs indicate that eight T_2-weighted images were acquired to localize one specific slice for the DWI scans. Figure 1b shows the proton T_2-weighted image from slice 6, which was subsequently used for the DWI scans for calculation of the proton ADC map. This slice was chosen because it typically depicts both core and penumbra in the MCAO rat model (32).

Figure 2 shows a representative hyperpolarized ^{129}Xe CSI from one control animal. This image illustrates that the signal of hyperpolarized ^{129}Xe dissolved in brain tissue can be observed in both brain hemispheres, as shown previously (24).

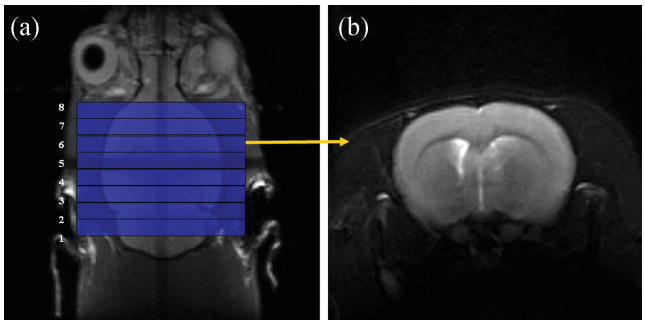

Figure 1. (a) Proton coronal image of a rat brain used for slice selection along the axial direction. Slice thickness, 2.5 mm. (b) Slice 6 was selected as a reference image.

Figure 3a shows a representative proton ADC map obtained 90 min following MCAO. There is a large ischemic core within the ipsilesional (right) MCA territory, as indicated by ADC values below the critical threshold of 5.3×10^{-4} mm^2/s for infarction (31). [The normal ADC value of rat brain tissue in the contralesional (left) hemisphere is $(7.5 \pm 1.8) \times 10^{-4}$ mm^2/s.] Figure 3b depicts the corresponding hyperpolarized ^{129}Xe CSI, indicating signal reduction in large parts of the right hemisphere, consistent with the area typically experiencing decreased CBF following right MCAO in the model used (20). Figure 3c shows the TTC-stained brain section of the same animal as illustrated in Fig. 3a, b; the black line in this figure delineates the infarcted brain tissue. Xenon CSI, shown in Fig. 3b, demonstrates reduced perfusion in brain tissue, ultimately leading to infarction, as shown by TTC staining in Fig. 3c. In Fig. 3d, the blue area represents the difference between the ADC lesion and TTC lesion areas, and the green area shows the nonischemic region.

ROI analyses were performed to further characterize the Xe CSI tissue signals within the different observed tissue compartments defined by their respective ADC and TTC signatures. Table 2 shows the xenon CSI signals for the defined ROIs from both MCAO and control groups. Xenon signals from each ROI in the contralesional (left) hemisphere were set as a reference (100%), and xenon signals from each ROI in the ipsilesional (right) hemisphere were normalized to these signals. The xenon signal in the ischemic core (ROI1) dropped to 8.4 ± 0.4% of the contralesional side signal, and the xenon signal in normal tissue (ROI2) remained the same. Moreover, the xenon signal in ROI1 was reduced significantly relative to the corresponding con-

Table 1. Physiological variables at different time points after middle cerebral artery occlusion (MCAO). For clarity, only data from two representative time points are shown

		MCAO group				Control group	
	Time	Rat 1	Rat 2	Rat 3	Rat 4	Rat 5	Rat 6
S_pO_2 (%)	Immediately after MCAO	95	96	96	95	95	96
	Mean ± SD		95.5 ± 0.6			95.5 ± 0.7	
	90 min	96	96	97	96	96	95
	Mean ± SD		96.3 ± 0.5			95.5 ± 0.7	
Heart rate	Immediately after MCAO	366	372	359	361	366	358
(beat per min)	Mean ± SD		364.5 ± 5.8			362 ± 5.7	
	90 min	358	369	362	360	363	356
	Mean ± SD		362.3 ± 4.8			359.5 ± 4.9	

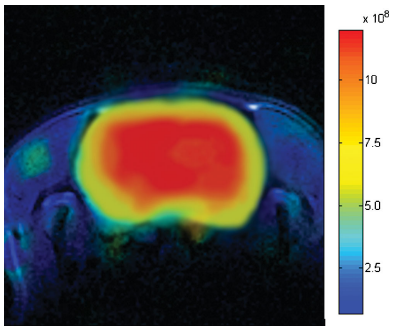

Figure 2. Hyperpolarized ^{129}Xe chemical shift imaging (CSI) from a nonlesioned rat brain (control experiment). A homogeneous hyperpolarized ^{129}Xe signal can be observed within both brain hemispheres. Xenon signal intensity is indicated in arbitrary units.

tralesional ROIs in the MCAO group, as well as the corresponding ipsilateral ROIs in control animals. Within the control group, no significant differences in the xenon signal were observed between the corresponding ROIs of both hemispheres.

DISCUSSION

As a result of the low concentration of xenon dissolved in brain tissue, it is impossible to obtain MR images with thermal polarization. Hyperpolarization is required to provide sensitivity, but the magnetization density of xenon in the dissolved phase is not sufficiently high for frequency-encoding imaging methods, such as gradient echo imaging. Hyperpolarization performed after the excitation pulse is nonrecoverable, whereas proton thermal polarization can be recovered during TR in conventional MR imaging. Therefore, we chose CSI to obtain xenon images. Because fresh hyperpolarized xenon was continuously delivered by CBF during all phase-encoding steps, the short T_1 for dissolved xenon was not a problem for the CSI modality. In general, the T_2 of dissolved xenon is short, and so this modality has an issue which limits the signal-to-noise ratio; however, using the CSI sequence, as the effective TE is 0.9 ms, the T_2^* of 17 ms allows for adequate time to collect the signal. As the T_2 values of dissolved xenon are generally short, we used a CSI sequence exactly for this reason, because it has a very short effective TE. To obtain a reference image for coregistration of the hyperpolarized ^{129}Xe MRI, we selected the slice with the same center as used for proton DWI. The polarization of hyperpolarized ^{129}Xe might vary over experiments; therefore, we set the xenon signal in

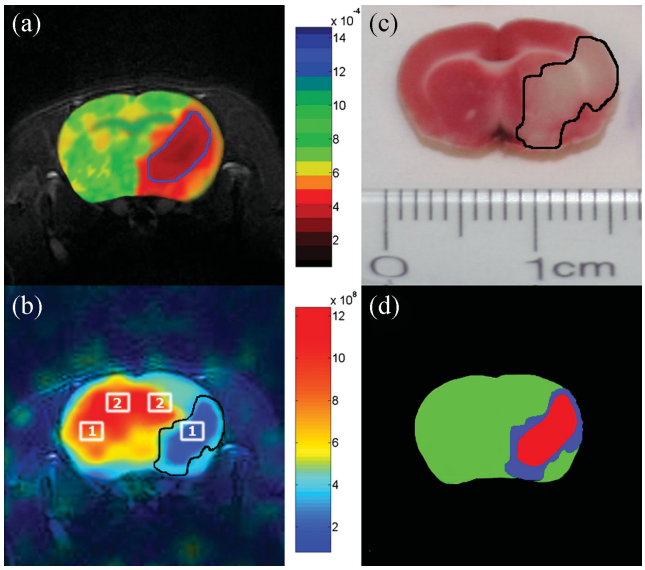

Figure 3. (a) Representative proton apparent diffusion coefficient (ADC) map image obtained 90 min after right middle cerebral artery occlusion (MCAO). The ischemic core is indicated by ADC values below 5.3×10^{-4} mm^2/s (circled by a blue line). (b) Corresponding hyperpolarized ^{129}Xe chemical shift image (CSI). There is a large signal void in the ipsilesional (right) hemisphere. The defined regions of interest (ROIs) are labeled as follows: ROI1, core; ROI2, normal tissue. The xenon signal intensity is given in arbitrary units. (c) Corresponding 2,3,5-triphenyltetrazolium chloride (TTC)-stained brain section of the same animal as in (a) and (b). (d) Tricolor map based on the ADC and TTC images shown in (a) and (c). Green, red and blue represent non-ischemic tissue, core and penumbra, respectively.

normal tissue as a reference in each experiment. This normalization enables xenon signal intensity data from ROIs in the lesioned hemisphere to be quantified and analyzed statistically with greater validity and accuracy.

Following inhalation, xenon dissolves in the blood of the pulmonary capillary system and is then circulated to the brain, where it penetrates the blood–brain barrier and is distributed into brain tissue. Therefore, as long as CBF is not compromised, the xenon signal in whole brain tissue should remain relatively constant during ^{129}Xe inhalation. Indeed, a homogeneous xenon signal was observed in the brains of control rats without significant hemispheric side-by-side differences. However, the hyperpolarized ^{129}Xe signal was reduced significantly in the right occluded hemisphere of MCAO rats, which is similar to the results

Table 2. Xenon chemical shift imaging (CSI) signal in different regions of interest (ROIs) of the brain from both middle cerebral artery occlusion (MCAO) and control groups, and statistics between the contralesional and ipsilesional sides, and between the two groups. The xenon signal from each ROI of the contralesional brain hemisphere was set at 100% as a reference, and all signals from the ROIs of the ipsilesional hemisphere were normalized to the xenon signal of the contralesional side tissue

	MCAO group			Control group			
ROI	Contralesional (left side) (reference)	Ipsilesional (right side)	*P* (between sides)	Contralesional (left side) (reference)	Ipsilesional (right side)	*P* (between sides)	*p* (between groups)
ROI1 (core)	100%	$8.4 \pm 0.4\%$	1.18×10^{-9}	100%	$99.9 \pm 0.2\%$	0.500	< 0.05
ROI2 (normal tissue)	100%	$99.6 \pm 0.3\%$	0.058	100%	$99.8 \pm 0.2\%$	0.344	> 0.05

reported previously for conventional proton PWI imaging (22,26). The dissipation of the xenon signal, which takes place in the extracellular space during the experiment, does not compromise the measurement of blood perfusion using the xenon signal intensity. First, we used a 90° radiofrequency pulse to acquire each phase encoding the CSI datum. Because the hyperpolarization of xenon is completely depolarized during each acquisition, we could not detect the residual magnetization of depolarized xenon. Second, because xenon's diffusion coefficient in water is 2.2×10^{-5} cm^2/s (33), it diffuses about 0.05 mm in 1 s. The xenon diffusion coefficient in brain tissue should be smaller because brain tissue has a higher viscosity than pure water. Even compared with proton diffusion imaging with a resolution of about 0.2 mm, diffusion is not a problem. Third, as xenon in tissue has a shorter T_1 than in the gas phase, its signal decays much more quickly. Only fresh hyperpolarized xenon arising from the blood flow contributes to the CSI signal. Therefore, xenon dissipation was not a problem in our experiment.

In two studies (34,35), Kohno *et al.* demonstrated nearly identical relative hemispheric lesion volumes at 2 and 7 h, respectively. Previously, we have evaluated the spatiotemporal evolution of the respective CBF and ADC lesions in the MCAO model, and found that substantial growth of the ischemic core occurs early following MCAO. However, this process is substantial slowed in permanent MCAO after the 60–90-min time point (26,36). After this time, there is no ADC–CBF mismatch identified, and the respective CBF and ADC lesion volumes essentially match the 24-h TTC volume (26,36). For the TTC volume, previous studies have shown that a 'maturation time' of as little as 6 h is sufficient to allow for the correct delineation of infarct size. Therefore, our choice of acquisition of ADC and xenon CSI at 90 min and waiting 8 h prior to TTC staining appear to be appropriate.

Xenon CSIs were interpreted from a raw data matrix of 16×16, which is not sufficient to show perfusion-like anatomical features produced by ASL or other perfusion methods. In our current experiment, xenon polarization was only about 10%. However, a higher xenon polarization using recently introduced hyperpolarized technology (37) and new signal enhancement methodology (38) would increase the spatial resolution of the xenon dissolved phase. We would expect this to provide more sensitive hyperpolarized xenon MR brain images. The xenon perfusion image is able to provide information complementary to conventional proton diffusion maps to determine the penumbra area, without injection of gadolinium-based contrast agents. Generally, the ADC–PWI mismatch is used to operationally define the ischemic penumbra. Hyperpolarized xenon MRI may provide a novel means to characterize tissue perfusion and assess ischemic penumbra. Subsequent research, using higher spatial resolution xenon MR images, would be helpful for further quantitative validation of these findings.

To achieve more precise identification of the stroke penumbra from the core, it is important to develop a quantitative method to quantify the regional blood flow from hyperpolarized xenon images. If perfusion imaging via ASL was not available, this would avoid the need to localize the ischemic penumbra through the exposure of stroke patients to intravenous contrast agents, which pose the risk of contrast-associated nephrogenic systemic fibrosis. Xenon is a chemically inert gas, and an anesthetic in alveolar concentrations higher than 70%. However, in human studies with hyperpolarized xenon, there were no adverse events reported after performing more than 350 breath-hold experiments (39,40). Although the MR signal-to-noise ratio of hyperpolarized ^{129}Xe dissolved in brain tissue is not as high as that of protons, and thus fast xenon imaging could not be implemented on the brain using the conventional MRI method, the recently developed Hyper-SAGE approach provides a novel method to amplify the dissolved xenon signal by remote detection of the extracted xenon gas (38). Combining the additional sensitivity of hyperpolarized ^{129}Xe to blood oxygenation and the xenon biosensor techniques developed (41–43), hyperpolarized xenon MRI is likely to have many important clinical applications in the future.

CONCLUSION

For the first time, we have shown that *in vivo* hyperpolarized ^{129}Xe MRI is able to detect an area of decreased CBF induced by MCAO. These preliminary results demonstrate the feasibility of detecting stroke by imaging hyperpolarized xenon in the brain tissue. More importantly, our results indicate the possibility of the use of *in vivo* MRI to diagnose brain disease employing inhaled hyperpolarized gas, eliminating the potential adverse effects to the patient resulting from the injection of gadolinium-based contrast agents.

Acknowledgements

XZ was supported by a grant from Wuhan Institute of Physics and Mathematics for the 'Hundred Talents Program' of the Chinese Academy of Sciences. This work was funded in part by a grant from the National Aeronautics and Space Administration (NASA) to MA (NAG9-1469). The xenon polarizer was provided by a loan agreement from General Electric Healthcare (Durham, NC, USA).

REFERENCES

1. Rosamond W, Flegal K, Furie K, Go A, Greenlund K, Haase N, Hailpern SM, Ho M, Howard V, Kissela B, Kittner S, Lloyd-Jones D, McDermott M, Meigs J, Moy C, Nichol G, O'Donnell C, Roger V, Sorlie P, Steinberger J, Thom T, Wilson M, Hong Y. Heart disease and stroke statistics – 2008 update: a report from the American Heart Association Statistics Committee and Stroke Statistics Subcommittee. Circulation 2008; 117(4): e25–146.
2. Fieschi C, Fisher M. *Prevention of Ischemic Stroke*, 1st edn. Informa Healthcare: London, 1999.
3. Mukherji SK, Chenevert TL, Castillo M. Diffusion-weighted magnetic resonance imaging. J. Neuroophthalmol. 2002; 22(2): 118–122.
4. Chien D, Kwong KK, Gress DR, Buonanno FS, Buxton RB, Rosen BR. MR diffusion imaging of cerebral infarction in humans. Am. J. Neuroradiol. 1992; 13(4): 1097–1102.
5. Calamante F, Thomas DL, Pell GS, Wiersma J, Turner R. Measuring cerebral blood flow using magnetic resonance imaging techniques. J. Cereb. Blood Flow Metab. 1999; 19(7): 701–735.
6. Ostergaard L, Sorensen AG, Kwong KK, Weisskoff RM, Gyldensted C, Rosen BR. High resolution measurement of cerebral blood flow using intravascular tracer bolus passages. Part II: Experimental comparison and preliminary results. Magn. Reson. Med. 1996; 36(5): 726–736.
7. Fisher M. The Ischemic Penumbra: A New Opportunity for Neuroprotection. Cerebrovasc Dis. 2006; 21(Suppl. 2): 64–70.
8. Davis S, Fisher M, Warach S. *Magnetic Resonance Imaging in Stroke*, 1st edn. Cambridge University Press: Cambridge, 2003.
9. Back T, Hoehn-Berlage M, Kohno K, Hossmann KA. Diffusion nuclear magnetic resonance imaging in experimental stroke. Correlation with cerebral metabolites. Stroke 1994; 25(2): 494–500.
10. Busza AL, Allen KL, King MD, van BN, Williams SR, Gadian DG. Diffusion-weighted imaging studies of cerebral ischemia in gerbils. Potential relevance to energy failure. Stroke 1992; 23(11): 1602–1612.

11. Warach S, Dashe JF, Edelman RR. Clinical outcome in ischemic stroke predicted by early diffusion-weighted and perfusion magnetic resonance imaging: a preliminary analysis. J. Cereb. Blood Flow Metab. 1996; 16(1): 53–59.
12. Sun PZ, Zhou J, Sun W, Huang J, van Zijl PC. Detection of the ischemic penumbra using pH-weighted MRI. J. Cereb. Blood Flow Metab. 2007; 27(6): 1129–1136.
13. Zhou J, Payen JF, Wilson DA, Traystman RJ, van Zijl PC. Using the amide proton signals of intracellular proteins and peptides to detect pH effects in MRI. Nat. Med. 2003; 9(8): 1085–1090.
14. Wertman R, Altun E, Martin DR, Mitchell DG, Leyendecker JR, O'Malley RB, Parsons DJ, Fuller ER III, Semelka RC. Risk of nephrogenic systemic fibrosis: evaluation of gadolinium chelate contrast agents at four American universities. Radiology 2008; 248(3): 799–806.
15. Grobner T. Gadolinium – a specific trigger for the development of nephrogenic fibrosing dermopathy and nephrogenic systemic fibrosis? Nephrol. Dial. Transplant. 2006; 21(4): 1104–1108.
16. Marckmann P, Skov L, Rossen K, Dupont A, Damholt MB, Heaf JG, Thomsen HS. Nephrogenic systemic fibrosis: suspected causative role of gadodiamide used for contrast-enhanced magnetic resonance imaging. J. Am. Soc. Nephrol. 2006; 17(9): 2359–2362.
17. Broome DR, Girguis MS, Baron PW, Cottrell AC, Kjellin I, Kirk GA. Gadodiamide-associated nephrogenic systemic fibrosis: why radiologists should be concerned. Am. J. Roentgenol. 2007; 188(2): 586–592.
18. Albert MS, Cates GD, Driehuys B, Happer W, Saam B, Springer CS Jr, Wishnia A. Biological magnetic resonance imaging using laser-polarized ^{129}Xe. Nature 1994; 370(6486): 199–201.
19. Duhamel G, Choquet P, Leviel JL, Steibel J, Lamalle L, Julien C, Kober F, Grillon E, Derouard J, Decorps M, Ziegler A, Constantinesco A. In vivo ^{129}Xe NMR in rat brain during intra-arterial injection of hyperpolarized ^{129}Xe dissolved in a lipid emulsion. C.R. Acad. Sci. III 2000; 323(6): 529–536.
20. Duhamel G, Choquet P, Grillon E, Leviel JL, Decorps M, Ziegler A, Constantinesco A. Global and regional cerebral blood flow measurements using NMR of injected hyperpolarized xenon-129. Acad. Radiol. 2002; 9 (Suppl 2): S498–S500.
21. Walker TG, Happer W. Spin-exchange optical pumping of noble-gas nuclei. Rev. Mod. Phys. 1997; 69: 629–642.
22. Zhou X, Luo J, Sun X, Zeng X, Ding S, Liu M, Zhan M. Enhancement of solid-state proton NMR via the spin-polarization-induced nuclear Overhauser effect with laser-polarized xenon. Phys. Rev. B 2004; 70: 052405-1–052405-4.
23. Zhou X, Sun X, Luo J, Zeng X, Liu M, Zhan M. Production of hyperpolarized ^{129}Xe gas without nitrogen by optical pumping at ^{133}Cs D_2 line in flow system. Chin. Phys. Lett. 2004; 21: 1501–1503.
24. Zhou X, Mazzanti ML, Chen JJ, Tzeng YS, Mansour JK, Gereige JD, Venkatesh AK, Sun Y, Mulkern RV, Albert MS. Reinvestigating hyperpolarized $^{(129)}$Xe longitudinal relaxation time in the rat brain with noise considerations. NMR Biomed. 2008; 21(3): 217–225.
25. Longa EZ, Weinstein PR, Carlson S, Cummins R. Reversible middle cerebral artery occlusion without craniectomy in rats. Stroke 1989; 20(1): 84–91.
26. Henninger N, Sicard KM, Schmidt KF, Bardutzky J, Fisher M. Comparison of ischemic lesion evolution in embolic versus mechanical middle cerebral artery occlusion in Sprague Dawley rats using diffusion and perfusion imaging. Stroke 2006; 37(5): 1283–1287.
27. Bouley J, Fisher M, Henninger N. Comparison between coated vs. uncoated suture middle cerebral artery occlusion in the rat as assessed by perfusion/diffusion weighted imaging. Neurosci. Lett. 2007; 412(3): 185–190.
28. Nakamura K, Kondoh Y, Wakai A, Kershaw J, Wright D, Kanno I. ^{129}Xe spectra from the heads of rats with and without ligation of the external carotid and pterygopalatine arteries. Magn. Reson. Med. 2005; 53(3): 528–534.
29. Wong EC, Cox RW, Song AW. Optimized isotropic diffusion weighting. Magn. Reson. Med. 1995; 34(2): 139–143.
30. Stejskal EO, Tanner JE. Spin diffusion measurements: spin echoes in the presence of a time-dependent field gradient. J. Chem. Phys. 1965; 42: 288–292.
31. Meng X, Fisher M, Shen Q, Sotak CH, Duong TQ. Characterizing the diffusion/perfusion mismatch in experimental focal cerebral ischemia. Ann. Neurol. 2004; 55(2): 207–212.
32. Bardutzky J, Shen Q, Henninger N, Bouley J, Duong TQ, Fisher M. Differences in ischemic lesion evolution in different rat strains using diffusion and perfusion imaging. Stroke 2005; 36(9): 2000–2005.
33. Wolber J, Doran SJ, Leach MO, Bifone A. Measuring diffusion of xenon in solution with hyperpolarized ^{129}Xe NMR. Chem. Phys. Lett. 1998; 296: 391–396.
34. Kohno K, Hoehn-Berlage M, Mies G, Back T, Hossmann KA. Relationship between diffusion-weighted MR images, cerebral blood flow, and energy state in experimental brain infarction. Magn. Reson. Imaging 1995; 13(1): 73–80.
35. Kohno K, Back T, Hoehn-Berlage M, Hossmann KA. A modified rat model of middle cerebral artery thread occlusion under electrophysiological control for magnetic resonance investigations. Magn. Reson. Imaging 1995; 13(1): 65–71.
36. Bardutzky J, Shen Q, Henninger N, Schwab S, Duong TQ, Fisher M. Characterizing tissue fate after transient cerebral ischemia of varying duration using quantitative diffusion and perfusion imaging. Stroke 2007; 38(4): 1336–1344.
37. Ruset IC, Ketel S, Hersman FW. Optical pumping system design for large production of hyerpolarization ^{129}Xe. Phys. Rev. Lett. 2006; 96(5): 053002-1–053002-4.
38. Zhou X, Graziani D, Pines A. Hyperpolarized xenon NMR and MRI signal amplification by gas extraction. Proc. Natl. Acad. Sci. USA 2009; 106: 16,903–16,906.
39. Loring SH, Butler JP, Patz S. Science to practice: how do we interpret the transfer of hyperpolarized ^{129}Xe from blood into alveolar gas? Radiology 2009; 252(2): 319–321.
40. Patz S, Hersman FW, Muradian I, Hrovat MI, Ruset IC, Ketel S, Jacobson F, Topulos GP, Hatabu H, Butler JP. Hyperpolarized $^{(129)}$Xe MRI: a viable functional lung imaging modality? Eur. J. Radiol. 2007; 64(3): 335–344.
41. Wolber J, Cherubini A, Leach MO, Bifone A. Hyperpolarized ^{129}Xe NMR as a probe for blood oxygenation. Magn. Reson. Med. 2000; 43(4): 491–496.
42. Schroder L, Lowery TJ, Hilty C, Wemmer DE, Pines A. Molecular imaging using a targeted magnetic resonance hyperpolarized biosensor. Science 2006; 314(5798): 446–449.
43. Driehuys B. Chemistry. Toward molecular imaging with xenon MRI. Science 2006; 314(5798): 432–433.